DOI: 10.1002/cmdc.200800311

Cytotoxic Rhodium(III) and Iridium(III) Polypyridyl Complexes: Structure–Activity Relationships, Antileukemic Activity, and Apoptosis Induction

Mara Dobroschke,[b] Yvonne Geldmacher,[a] Ingo Ott,[c] Melanie Harlos,[a] Lisa Kater,[b] Laura Wagner,[b] Ronald Gust,[c] William S. Sheldrick,*[a] and Aram Prokop[b]

Meridional rhodium(III) polypyridyl complexes of the type mer-*[RhX$_3$(DMSO)(pp)] (X = Cl, pp = phen* ***1****, dpq* ***2****, dppz* ***3****; X = Br, pp = phen* ***4****) represent a promising class of potent cytostatic agents for the treatment of lymphoma and leukemia. Exposure of their DMSO solutions to light leads to slow isomerization to mixtures of the* mer *and the generally less active* fac *isomers. As a result, the IC$_{50}$ values of* ***1*** *and* ***2*** *toward HT-29 cells increase from 0.19 and 0.069 μM on immediate use in the dark to 0.66 and 0.312 μM, respectively, after exposure of their DMSO stock solutions to light for 7 days. In striking contrast, the complexes* mer-*[IrX$_3$(DMSO)(phen)] (X = Cl* ***7****, Br* ***8****) are significantly less cytotoxic than their facial Ir^{III} polypyridyl counterparts: IC$_{50}$ = 20.3 μM for* ***7*** *and 4.6 μM for* fac-*[IrCl$_3$(DMSO)(phen)]* ***5*** *toward MCF-7 cells. The IC$_{50}$ values for the complexes* fac-*[IrX$_3$(L)(pp)]* ***9–13*** *decrease in the orders: a) Cl > Br for X and b) H$_2$O > DMSO for L. Specific apoptotic cell death by DNA fragmentation was detected for leukemia (NALM-6) and lymphoma (BJAB) cells after incubation with* ***2****,* ***3****, and* ***11*** *(X = Br, L = H$_2$O, pp = phen) for 72 h. Loss of the mitochondrial membrane potential in lymphoma cells indicates that apoptosis is mediated via the intrinsic mitochondrial pathway. LDH release assays after 1 or 3 h demonstrate that necrotic damage is negligible.*

Introduction

Although the anticancer properties of dirhodium(II,II) carboxylates are well established,[1–3] relatively few investigations have been carried out on the possible cytotoxic activity of rhodium(III) complexes. However, recent reports have suggested that octahedral chloridorhodium(III) complexes containing N-donor ligands could offer considerable scope for the development of anticancer agents. For instance, *mer,cis*-[RhCl$_3$(DMSO-κ*S*)$_2$(NH$_3$)] exhibits remarkable cytotoxicity (IC$_{50}$ = 1.5 ± 0.4, 0.4 ± 0.2, and 9 μM) toward the human cell lines A2780 (ovarian carcinoma), LoVo (colon carcinoma), and Calu (lung carcinoma), respectively.[4] High cytotoxic activity has also been established for *fac*-[RhCl$_3$([9]ane-NS$_2$)][5] ([9]ane-NS$_2$ = 1-aza-4,7-dithiacyclononane) and the terpyridine complexes[6] *mer*-[RhCl$_3$(tpy)] (tpy = 2,2′:6′,2″-terpyridine) and [Rh(Im)(tpy)$_2$]Cl$_3$·3H$_2$O (Im = imidazole).

We recently demonstrated that the cytotoxicities of organometallic Rh^{III} and Ir^{III} complexes of the type [(η^5-C$_5$Me$_5$)MCl(pp)](CF$_3$SO$_3$) (M = Rh, Ir) toward the human cell lines MCF-7 (breast cancer) and HT-29 (colon cancer) are directly correlated to the size of the polypyridyl ligand pp.[7,8] A similar dependence is observed for the analogous organoruthenium(II) complexes [(η^6-C$_6$Me$_6$)RuCl(pp)](CF$_3$SO$_3$).[9] These findings led us to investigate the biological properties of the trichloridorhodium(III) complexes *mer*-[RhCl$_3$(DMSO-κ*S*)(pp)] with the polypyridyl ligands pp = bpy, phen, dpq, dppz, dppn (bpy = 2,2-bipyridine; phen = 1,10-phenanthroline; dpq = dipyrido[3,2-*f*:2′,3′-*h*]quinoxaline; dppz = dipyrido[3,2-*a*:2′,3′-*c*]phenazine; dppn = benzo[*i*]dipyrido[3,2-*a*:2′,3′-*c*]phenazine). Such complexes are extremely potent in vitro cytotoxic agents and exhibit IC$_{50}$ values that are once again strongly dependent on the size of the polypyridyl ligand: 1.9 ± 0.5, 0.19 ± 0.05, and 0.069 ± 0.021 μM against the HT-29 cell line respectively for pp = bpy, phen, dpq.[10] A remarkable feature of these meridional complexes is their very high level of cellular uptake relative to other established metallodrugs. For instance, *mer*-[RhCl$_3$(DMSO-κ*S*)(dpq)] is accumulated some 102-fold in HT-29 cells (53.6 ng Rh per mg cell protein) with respect to the exposure concentration of 1.0 μM. In striking contrast, no significant cell uptake was observed for the same exposure concentration of the facial complexes *fac*-[IrCl$_3$(DMSO-κ*S*)(pp)] (pp = bpy, phen, dpq), which exhibit much lower IC$_{50}$ values of > 100, 4.6 ± 0.2, and 6.1 ± 0.7 μM toward HT-29 cells.[11] Although stable in aqueous and methanol solutions, the facial iridium(III) complexes do rapidly isomerize to a mixture of *fac* and *mer* isomers in CH$_2$Cl$_2$ solution on exposure to light. The meridional rhodium(III) complexes *mer*-[RhCl$_3$(DMSO-κ*S*)(pp)] are, in contrast, stable in CH$_2$Cl$_2$ solution but undergo photochemical isomerization in

[a] *Y. Geldmacher, M. Harlos, Prof. Dr. W. S. Sheldrick*
Lehrstuhl für Analytische Chemie
Ruhr-Universität Bochum, 44780 Bochum (Germany)
Fax: (+49) 234-321 4420
E-mail: william.sheldrick@rub.de

[b] *M. Dobroschke, L. Kater, L. Wagner, Dr. A. Prokop*
Department of Pediatric Oncology/Hematology
University Medial Center Charité Berlin, 13353 Berlin (Germany)

[c] *Dr. I. Ott, Prof. Dr. R. Gust*
Institut für Pharmazie, Freie Universität Berlin
Königin-Luise-Straße 2–4, 14195 Berlin (Germany)

Supporting information for this article is available on the WWW under http://dx.doi.org/10.1002/cmdc.200800311.

polar solvents to an equilibrium mixture of *fac* and *mer* isomers.

To establish structure–activity relationships and to clarify the nature of the active species, we have now studied the influence of a) the geometry (*mer* vs. *fac*), b) the monodentate ligand L, and c) the anionic ligands X in complexes of the type *mer*- and *fac*-[MX_3(L)(pp)] (M = Rh, Ir; X = Cl, Br; pp = phen, dpq) toward the cell lines MCF-7 and HT-29. The cytotoxic activity of the previously characterized highly cytotoxic complexes *mer*-[$RhCl_3$(DMSO-κ*S*)(pp)] (pp = dpq **2**, dppz **3**) as well as *fac*-[$IrBr_3(H_2O)$(phen)] **11** and *mer*-[$IrCl_3$(tpy)] **14** was also evaluated in vitro toward Burkitt-like lymphoma cells (BJAB). Further experiments were performed for these active complexes to assess the relative importance of necrosis and apoptosis for the observed cell death and whether the intrinsic mitochondrial pathway is involved.

Results and Discussion

Synthesis and structure

We previously reported[10] the synthesis of the rhodium(III) polypyridyl complexes *mer*-[$RhCl_3$(DMSO-κ*S*)(pp)] (pp = phen, dpq, dppz, **1**–**3**) (Figure 1) as well as the analogous bpy and

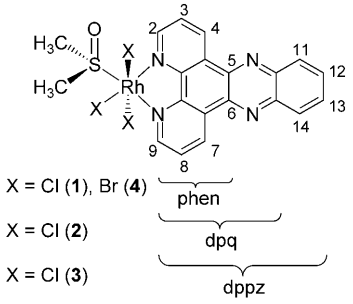

Figure 1. Meridional rhodium(III) complexes *mer*-[RhX_3(DMSO)(pp)].

dppn derivatives by treatment of the precursor *mer,cis*-[$RhCl_3$(DMSO-κ*S*)(DMSO-κ*O*)][12,13] with an equivalent of the appropriate polypyridyl ligand in a solution of CH_3OH/H_2O (1:1 *v/v*). A similar strategy was employed to synthesize the tribromorhodium(III) complex *mer*-[$RhBr_3$(DMSO-κ*S*)(phen)] **4** reported herein (Figure 1), in which the intermediate complex [$RhBr_3(DMSO)_3$] was produced by reaction of $RhBr_3 \cdot 3H_2O$ with three equivalents of DMSO and subsequently treated without further characterization with the appropriate polypyridyl ligand. This phen complex was chosen to study the possible influence of the anionic ligand X on the cytotoxicity of the meridional rhodium(III) polypyridyl compounds. The meridional structure of **4** was confirmed by the significant downfield shifts of protons H7 and H9 (0.05–0.07 ppm in DMSO solution) of the pyridine ring situated *trans* to the κ*S* DMSO ligand in comparison with H2 and H4 of the pyridine ring in *trans* position to a bromide ligand. Confirmation of the κ*S* coordination of the DMSO ligand was provided by the pronounced downfield shift of its methyl ^{1}H NMR resonance at 3.95 ppm in DMSO solution relative to the signal of free DMSO at 2.50 ppm. Analogous low-field values in the range 3.75–3.84 ppm were observed for the DMSO ligands in the trichloridorhodium(III) complexes **1**–**3**.[10]

Solutions of **4** in DMSO isomerize to mixtures of the *mer* and *fac* isomers on exposure to light. A *mer*/*fac* ratio of 69:31 is observed in DMSO solution after exposure to light for 15 min and an equilibrium ratio of 38:62 after 5 days. A marked upfield shift from two separate doublets at 10.21 and 10.26 ppm to a common doublet at 9.89 ppm is recorded for the H2 and H9 protons of **4** on isomerization to the C_s symmetrical *fac* isomer in which the protons H2/H9, H3/H8, H4/H7, and H5/H6 are magnetically equivalent. Slightly more rapid isomerization was reported for the trichlorido analogue[10] *mer*-[$RhCl_3$(DMSO)(phen)] **1**, for which a *mer*/*fac* ratio of 60:40 is present in DMSO after 15 min irradiation with ambient light and a lower percentage of the *mer* isomer in the equilibrium ratio of 30:70 after 5 days (Figure 2).

A slower isomerization is observed for DMSO solutions of the dpq and dppz complexes **2** and **3** in the presence of light. For instance, whereas a 10 mM solution of the dpq complex **2** exhibits a *mer*/*fac* ratio of about 75:25 after 24 h, this slowly reverses to an equilibrium mixture at about 39:61 after 5 days. Values of 63:37 and 50:50 are observed for the *mer*/*fac* ratio in a 2.5 mM solution of the less soluble dppz complex **3** after 24 h and 5 days, respectively. Attempts to prepare facial trichloridorhodium(III) complexes of the type *fac*-[$RhCl_3$(DMSO-κ*S*)(pp)] in a manner similar to that employed for the analogous iridium(III) complexes[11] by stepwise reaction of $RhCl_3 \cdot 3H_2O$ with the appropriate polypyridyl ligand and DMSO in aqueous or methanol solution in the dark led invariably to mixtures of the *fac* and *mer* isomers. The observed *mer*/*fac* ratios for the resulting mixtures in DMSO solution were similar to those recorded after irradiation of the *mer* complexes by daylight for 5 days. Mixtures of *fac* and *mer* isomers were also obtained for the aqua precursors of the type [$RhCl_3$-(H_2O)(pp)].[14]

Meridional iridium(III) complexes of the type *mer*-[IrX_3-(DMSO-κ*S*)(phen)] (X = Cl, **7**; X = Br, **8**) (Figure 3) were prepared in an analogous manner to their rhodium(III) counterparts, and facial iridium(III) complexes of the types *fac*-[$IrCl_3(H_2O)$(pp)] (pp = phen, **9**; pp = dpq, **10**) and *fac*-[$IrBr_3$(L)(phen)] (L = H_2O, **11**; L = 1-MeIm, 1-methylimidazole, **12**; L = 1-MeBIm, 1-methylbenzimidazole, **13**) (Figure 4) by reaction of $IrCl_3 \cdot 3H_2O$ with the appropriate polypyridyl ligand in aqueous solution followed by the ligand L where necessary (for **12** and **13**). The respective meridional and facial ligand arrangements were confirmed by the ^{1}H NMR spectra of the complexes in the dark. Figure 5 depicts the aromatic region of the ^{1}H NMR spectrum of *mer*-[$IrBr_3$-(DMSO)(phen)] **8**, which together with its trichlorido counterpart **7** is indefinitely stable in $CDCl_3$ solution in the dark. Very slow isomerization to a mixture of *mer* and *fac* isomers is observed for **7** and **8** in DMSO solution with exposure to ambient light. After 24 h, respective *mer*/*fac* ratios of 91:9 and 89:11 are recorded, which decrease to 83:17 and 81:19 after 5 days. The preparation of both "*mer*" and "*fac*" complexes of the type [$IrX_3(H_2O)$(phen)] (X = Cl, Br) by solvent removal from aqueous

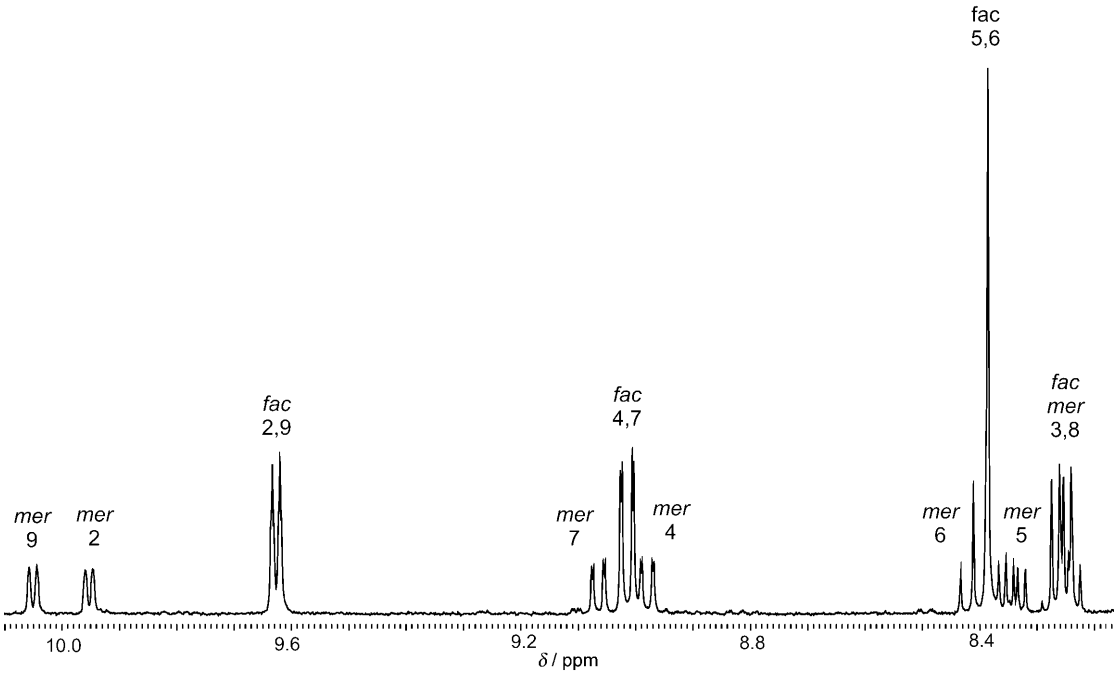

Figure 2. Aromatic region of the ^{1}H NMR spectrum of *mer*-[$RhCl_3$(DMSO)(phen)] **1** in DMSO after exposure to ambient light for 5 days.

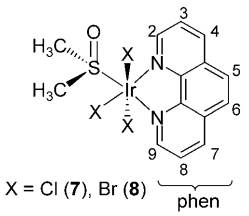

Figure 3. Meridional iridium(III) complexes *mer*-[IrX_3(DMSO)(phen)].

solutions of the $[IrX_4(phen)]^-$ anions with hydronium and ammonium counter-cations, respectively, was previously reported,[15] but the assignments were based solely on IR data and remain tentative.

As reported previously for the complexes *fac*-[$IrCl_3$(DMSO)(pp)] (pp = bpy, phen, dpq, dppz, dppn),[11] the facial iridium(III) complexes **9**–**13** are stable in D_2O or CD_3OD solution in the presence of light, but slowly isomerize to *fac*/*mer* mixtures in DMSO solution. Although we were unsuccessful in obtaining single crystals of these compounds suitable for X-ray analysis, the facial arrangement could be confirmed for *fac*-[$IrCl_3$(CH_3CN-κ*N*)(phen)] **9a**. Suitable crystals of this compound, the molecular structure of which is depicted in Figure 6, were isolated by slow evaporation of a solution of *fac*-[$IrCl_3$(H_2O)(phen)] **9** in acetonitrile.[16] The formation of **9a** is in accordance with the previously reported ability of the facial trichloridoiridium(III) complexes to replace their neutral monodentate ligand L by softer alternatives, for example, DMSO by *N*-acetylmethionine in the case of *fac*-[$IrCl_3$-(DMSO-κ*S*)(dppz)].[11]

The novel meridional iridium(III) complexes *mer*-[IrX_3(tpy)] (X = Cl, **14**; X = Br, **15**) were prepared by reaction of $IrX_3 \cdot 3H_2O$ with 2,2′:6′,2″-terpyridine in methanol and were included in the investigations for comparison purposes. Compounds **14** and **15** are isostructural[17,18] and crystallize in the monoclinic space group $P2_1/n$, in contrast to the triclinic compound *mer*-[$RhCl_3$(tpy)]·DMSO.[6] The molecular structure of **14** is depicted in Figure 7 and shows that the tridentate coordination mode of the tpy ligand leads to significant distortions in the basically octahedral environment of the iridium atom Ir1. Whereas the bond angles of Cl1–Ir1–Cl2 and N2–Ir1–Cl3 (respectively 179.51(3) and 177.34(8)°) are both close to the ideal angle of

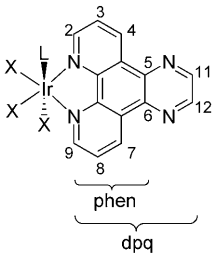

Figure 4. Facial iridium(III) complexes *fac*-[IrX_3(L)(pp)].

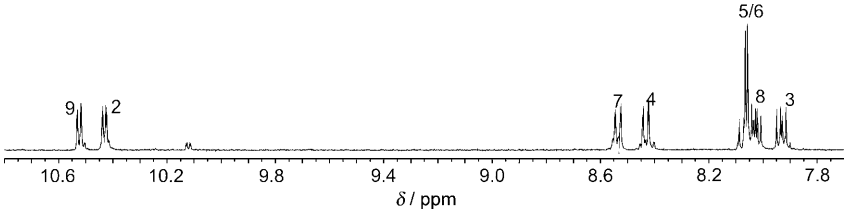

Figure 5. Aromatic region of the ^{1}H NMR spectrum of *mer*-[$IrBr_3$(DMSO)(phen)] **8** in $CDCl_3$ in the dark after 3 weeks.

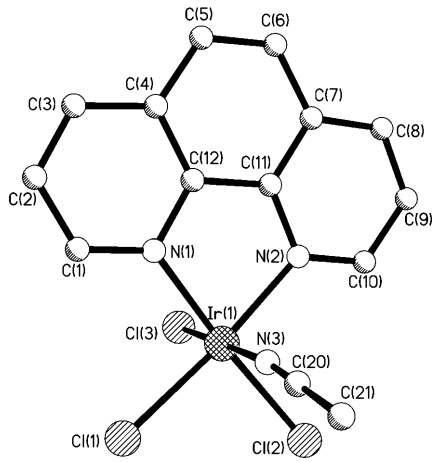

Figure 6. Molecular structure of *fac*-[$IrCl_3(CH_3CN)$(phen)] **9a**. Selected bond distances (Å): Ir1–N1 2.042(4), Ir1–N2 2.048(3), Ir1–N3 2.005(4), Ir1–Cl1 2.352(1), Ir1–Cl2 2.358(1), Ir1–Cl3 2.340(1).

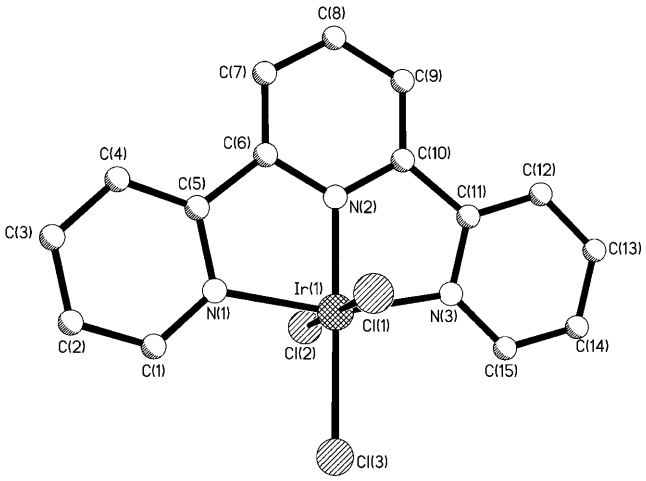

Figure 7. Molecular structure of *mer*-[$IrCl_3$(tpy)] **14**. Selected bond distances (Å): Ir1–N1 2.044(3), Ir1–N2 1.927(3), Ir–N3 2.049(3), Ir1–Cl1 2.356(1), Ir1–Cl2 2.347(1), Ir1–Cl3 2.370(1).

180°, that of N1–Ir1–N3 is much smaller (161.34(12)°) owing to the participation of Ir1 in two strained five-membered chelate rings. The central Ir1–N2 bond length of 1.927(3) Å is significantly shorter than the Ir1–N1 and Ir1–N3 distances of 2.044(3) and 2.049(3) Å, and this leads to a lengthening of the *trans* sited Ir1–Cl3 bond to 2.370(1) relative to the other Ir1–Cl distances of 2.356(1) (Ir1–Cl1) and 2.347(1) Å (Ir1–Cl2).

Cytotoxicity and structure–activity relationships

Table 1 lists the in vitro cytotoxicity of the rhodium(III) complexes **1**–**4** against the human cancer cell lines MCF-7 and HT-29 after respective incubation periods of 96 and 72 h. Equilibrium mixtures *fac*/*mer*-[$RhCl_3$(DMSO)(pp)] (pp = phen, **1a**; dpq **2a**; dppz **3a**) predominantly containing the *fac* isomer were obtained by exposing DMSO solutions of **1**–**3** to light for 7 days. The marked increases in the IC_{50} values for the irradiated DMSO solutions of **1a** and **2a** suggest that the *fac* isomers must exhibit a significantly lower cytotoxicity than their *mer* counterparts. An analogous, yet less pronounced, decrease in activity is also observed for the DMSO solutions of *mer*-[$RhCl_3$(DMSO)(pp)] (pp = bpy, dppn) after light exposure for a similar period of time. Surprisingly, no significant change in cytotoxicity is detected for the equilibrium mixture *fac*/*mer*-[$RhCl_3$(DMSO)(dppz)] **3a** in comparison with *mer*-[$RhCl_3$(DMSO)(dppz)] alone. The rate of the *mer*→*fac* isomerization and the value of the *fac*/*mer* ratio after 7 days are somewhat lower for the tribromido complex **4** relative to its trichlorido analogue **1**. Therefore, it can be postulated that the increased kinetic stability of the more active meridional isomer could be responsible for the slightly lower IC_{50} values of 0.203 and 0.091 μM for **4** toward MCF-7 and HT-29 cells relative to those of 0.40 and 0.19 μM recorded for **1**. Isomerization of the trihalogenido complexes *mer*-[$RhCl_3$(DMSO-κ*S*)(pp)] in DMSO can, in principle, proceed by either a multistep dissociation/coordination process or by a concerted interchange pathway involving a 7-coordinated transition state. Second-order kinetics[19,20] have been reported for both water substitution in [$(\eta^5$-$C_5Me_5)$Ir(phen)$(H_2O)]^{2+}$ and chloride substitution in [$(\eta^6$-$C_6H_6)$RuCl(en)]$^+$. Whereas activation parameters support an interchange dissociative pathway (I_d) in the former case, density functional calculations suggest that the interchange pathway would be more associative in the latter case. This shift in the $I_d \leftrightarrow I_a$ mechanistic continuum is in accordance with the marked decrease in the *trans* effect of the η^6-C_6H_6 ligand in comparison with [η^5-$C_5Me_5]^-$. In view of the low *trans* effects of the halogenide and polypyridyl N donor ligands it seems probable that a more associative interchange pathway will also

Table 1. Inhibitory activity of rhodium(III) polypyridyl complexes toward the human cell lines MCF-7 and HT-29.

	Complex	IC_{50} [μM][a] MCF-7	HT-29
	mer-[$RhCl_3$(DMSO)(bpy)][10]	4.0 ± 0.5	1.9 ± 0.5
1[10]	*mer*-[$RhCl_3$(DMSO)(phen)]	0.40 ± 0.06	0.19 ± 0.05
2[10]	*mer*-[$RhCl_3$(DMSO)(dpq)]	0.079 ± 0.012	0.069 ± 0.021
3[10]	*mer*-[$RhCl_3$(DMSO)(dppz)]	0.095 ± 0.020	0.073 ± 0.017
	mer-[$RhCl_3$(DMSO)(dppn)][10]	0.051 ± 0.012	0.070 ± 0.008
4	*mer*-[$RhBr_3$(DMSO)(phen)]	0.203 ± 0.033	0.091 ± 0.011
	fac/*mer*-[$RhCl_3$(DMSO)(bpy)]	5.1 ± 1.3	4.0 ± 1.1
1a	*fac*/*mer*-[$RhCl_3$(DMSO)(phen)]	1.1 ± 0.2	0.66 ± 0.02
2a	*fac*/*mer*-[$RhCl_3$(DMSO)(dpq)]	0.474 ± 0.030	0.312 ± 0.032
3a	*fac*/*mer*-[$RhCl_3$(DMO)(dppz)]	0.093 ± 0.05	0.057 ± 0.021
	fac/*mer*-[$RhCl_3$(DMSO)(dppn)]	0.15 ± 0.05	0.21 ± 0.04

[a] Values for **1**–**4** and *mer*-[$RhCl_3$(DMSO)(pp)] (pp = bpy, dppn)[10] are for freshly prepared DMSO solutions in the dark, those for **1a**–**3a** and *fac*/*mer*-[$RhCl_3$(DMSO)(pp)] (pp = bpy, dppn) are for DMSO solutions of the compounds after ambient light irradiation for 7 days.

be adopted by the complexes *mer*-[RhX_3(DMSO)(pp)]. The presence of the larger bromide ligands in **4** will increase steric crowding in the required transition state and could, therefore, lead to the observed slowing in the rate of *mer*→*fac* isomerization.

In striking contrast to the rhodium(III) complexes, facial iridium(III) isomers are much more cytotoxic than their meridional counterparts **7** and **8** (Table 2), whose rather low activity (16.8–45.9 μM) precludes further discussion of their individual structure–activity relationship. The IC_{50} values for *fac*-[$IrCl_3$(DMSO)(phen)] toward MCF-7 and HT-29 cells are respectively 4.4- and 3.7-fold lower than for *mer*-[$IrCl_3$(DMSO)(phen)]. Whereas the latter isomer is some 51-fold less active toward MCF-7 cells and 187 times less active toward HT-29 than *mer*-[$RhCl_3$(DMSO)(phen)], the facial Ir^{III} and Rh^{III} isomers appear to exhibit rather similar cytotoxicities. IC_{50} values of 4.6 ± 0.5 (MCF-7) and 4.6 ± 0.2 μM (HT-29) were measured for *fac*-[$IrCl_3$(DMSO)(phen)] and 1.1 ± 0.2 and 0.66 ± 0.02 μM for the irradiated mixture *fac*/*mer*-[$RhCl_3$(DMSO)(phen)] **2a** containing a *fac*/*mer* ratio of about 70:30 on the basis of ^{1}H NMR studies. Two interesting structure–activity relationships can be established for the facial iridium(III) complexes on taking the IC_{50} values for the compound pairs *fac*-[$IrCl_3$(L)(phen)] (L = DMSO, **5**; H_2O, **9**) and *fac*-[$IrX_3(H_2O)$(phen)] (X = Cl, **9**; X = Br, **11**) into account. Firstly, the DMSO complex is significantly more cytotoxic ($IC_{50}=4.6\pm0.5$ and 4.6 ± 0.2 μM for MCF-7 and HT-29 cells) than its aqua counterpart **9** ($IC_{50}=14.8\pm1.4$, 12.6 ± 1.9 μM) and secondly, a similar increase in activity is observed for the aqua complexes **9** and **11** on going from X = Cl (**9**) to X = Br (**11**; $IC_{50}=5.5\pm0.3$, 4.3 ± 0.2 μM). The complexes *fac*-[$IrBr_3$(L)(phen)] (L = 1-MeIm **12**, L = 1-MeBIm **13**) exhibit IC_{50} values in the range 6.9–8.7 μM toward MCF-7 and HT-29 cells and are therefore slightly less active than the aqua complex **11**. The markedly lower activity of *fac*-[$IrCl_3(H_2O)$(phen)] **9** relative to the analogous DMSO complex **5** indicates that an intermediate hydrolysis step may not be involved in the mechanism of action of **5**. Indeed, no ^{1}H NMR evidence for DMSO/H_2O substitution was recorded for an aqueous solution of **5** over a period of 24 h. It is possible that the differences in cytotoxicity (H_2O < DMSO, Cl < Br) may be related to the extent of cellular uptake.

The inhibition of cell proliferation by complexes **2**, **3**, **11**, and **14** was also evaluated in vitro in BJAB cells (Burkitt-like lymphoma cells).[21] After an incubation period of 24 h, the viability and cell count were measured with a CASY Cell Counter and Analyzer System, with the settings specifically defined for the requirements of the employed cells. The dose-dependent decrease in cell proliferation is depicted for the highly potent rhodium(III) complexes **2** and **3** in Figure 8. ID_{50} values for these complexes and the iridium(III) complexes **11** and **14** are listed in Table 3. It is apparent that the meridional complexes **2**, **3**, and **14** are all effective at low-micromolar concentrations in inhibiting proliferation of the lymphoma cells (ID_{50} values: 0.4–0.8 μM). The facial iridium(III) complex **11** is also effective but at a significantly higher dose level ($ID_{50}=5$ μM).

Apoptosis induction

Necrotic cell death is characterized by the early release of lactate dehydrogenase (LDH), whereas apoptotic cells initially retain their membrane integrity and do not exhibit rapid release of large intracellular proteins such as LDH. Figure 9a depicts the LDH release established for BJAB cells after 1 h incubation with various concentrations of *fac*-[$IrBr_3(H_2O)$(phen)] (**11**) and *mer*-[$IrCl_3$(tpy)] (**14**). These results clearly indicate that the meridional tpy complex causes considerable unspecific damage within a short period of time, and is therefore unsuitable as an anticancer agent. In contrast, the facial complex **11** has no significant unspecific cytotoxic effects on BJAB cells even though the concentrations used (2–10 μM) were an order of magnitude higher than for **14**. This was also the case for the highly active rhodium(III) complexes *mer*-[$RhCl_3$(DMSO-κ*S*)(pp)] **2** and **3**, for which concentrations in the range 0.4–1.0 μM were employed for an incubation period of 3 h (Figure 9b). These results indicate that necrosis does not have a significant impact on the potency of the complexes **2**, **3**, and **11**.

Apoptosis, in contrast to unspecific necrosis, requires a controlled and regulated mechanism leading to cell death. DNA fragmentation (hypoploidy) is considered to be a typical effect of apoptotic cell death, and we therefore quantified the induction of apoptosis for **2**, **3**, **11**, and **14** by flow cytometric measurements of the DNA fragments after incubating lymphoma cells (BJAB) and other cell lines for 72 h with the complexes.[22] The amounts of apoptotic NALM-6 cells for various concentrations of **2** and **3** are illustrated in Figure 10a. Extensive DNA fragmentation is observed even at very low concentrations (0.3, 0.8 μM) used for the cytotoxic complexes. The in-

Table 2. Inhibitory activity of iridium(III) polypyridyl complexes toward the human cell lines MCF-7 and HT-29.

	Complex	IC_{50} [μM][a] MCF-7	HT-29
5[11]	*fac*-[$IrCl_3$(DMSO)(phen)]	4.6 ± 0.5	4.6 ± 0.2
6[11]	*fac*-[$IrCl_3$(DMSO)(dpq)]	5.5 ± 0.9	6.1 ± 0.7
7	*mer*-[$IrCl_3$(DMSO)(phen)]	20.3 ± 0.5	16.8 ± 0.1
8	*mer*-[$IrBr_3$(DMSO)(phen)]	32.3 ± 2.7	45.9 ± 5.4
9	*fac*-[$IrCl_3(H_2O)$(phen)]	14.8 ± 1.4	12.6 ± 1.9
10	*fac*-[$IrCl_3(H_2O)$(dpq)]	11.3 ± 0.1	10.6 ± 0.6
11	*fac*-[$IrBr_3(H_2O)$(phen)]	5.5 ± 0.3[b]	4.3 ± 0.2[b]
12	*fac*-[$IrBr_3$(1-MeIm)(phen)]	8.6 ± 2.2	8.7 ± 0.6
13	*fac*-[$IrBr_3$(1-MeBIm)(phen)]	8.4 ± 0.6[b]	6.9 ± 1.2[b]
14	*mer*-[$IrCl_3$(tpy)]	0.32 ± 0.07	0.13 ± 0.02
15	*mer*-[$IrBr_3$(tpy)]	0.33 ± 0.02	0.26 ± 0.06

[a] Values for **5**–**8** and **14**–**15** are for freshly prepared DMSO solutions, those for **9**–**13** are for freshly prepared DMF solutions. [b] Values of 4.5 ± 0.3 and 3.9 ± 1.0 μM were obtained for stock solutions of **11** in DMSO and 7.3 and 9.3 μM for stock solutions of **13** in DMSO (MCF-7 and HT-29 cells, respectively).

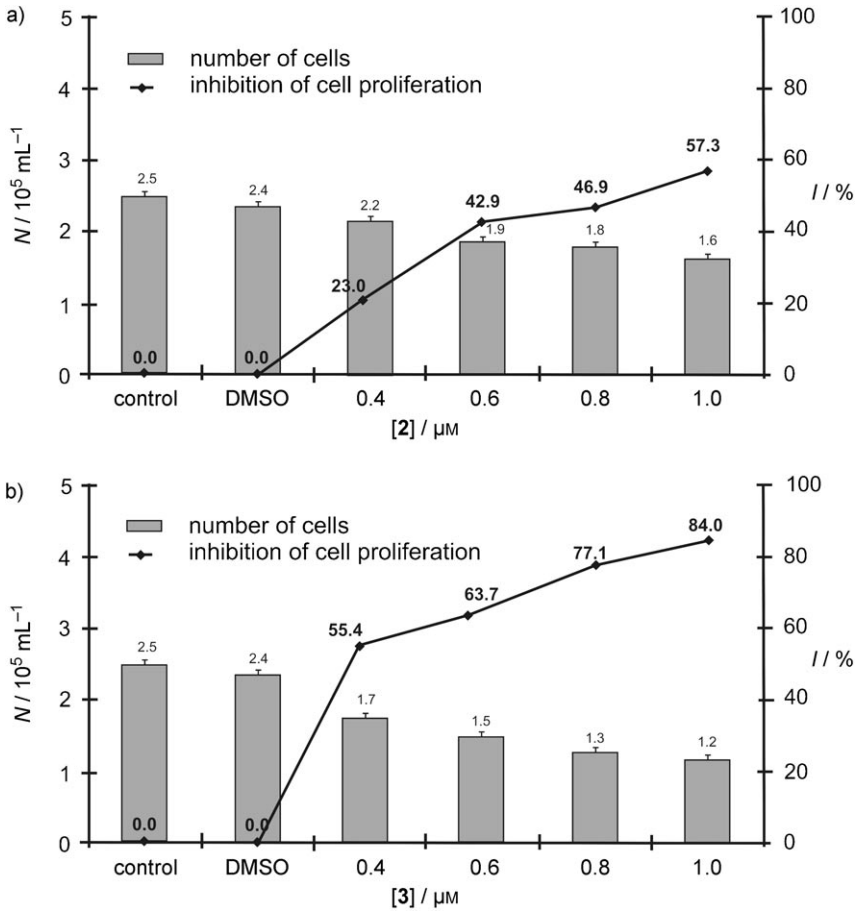

Figure 8. Inhibition of cell proliferation in Burkitt-like lymphoma cells after treatment with complexes a) **2** and b) **3** for 24 h as measured by a CASY cell counter (control = untreated cells). N = number of cells in units of 10^5 cells mL^{-1} ± ESD ($n = 3$); I = inhibition of cell proliferation with values given as percent of control values; 1×10^5 BJAB cells normally grow up to 2.5×10^5 cells mL^{-1} in 24 h in the absence of proliferation inhibitors.

Table 3. Biological data for complexes **2**, **3**, **11**, and **14** in BJAB cells.

Compd	ID_{50} [μM][a]	AC_{50} [μM][b]	c [μM][c]
2	0.8	1.2	0.8
3	0.4	1.0	0.6
11	5.0	40.0	25.0
14	0.5	0.6	4.0

[a] Inhibition of proliferation after 24 h. [b] Apoptosis induction after 75 h. [c] Dissipation of mitochondrial membrane potential ($\Delta\psi_m$), reported as the compound concentration giving 50% cells with low $\Delta\psi_m$ after 48 h.

duction of apoptosis in BJAB cells was also confirmed for the meridional trichloridorhodium(III) complexes (Figure 10 b) and this was also the case for the doxorubicin-resistant cell line 7CCA when treated with the dpq complex **2** but not the dppz complex **3**. After incubating BJAB cells with **3** for 12 h, significant changes could also be identified by fluorescence microscopy. The cell integrity is damaged (Supporting Information, figure S1) and the nucleus of the BJAB cells appears to be fragmented. The cells appear to have undergone apoptosis by shrinking and fragmentation.

Acute lymphoblastic leukemia (ALL) is the most common malignant disease in childhood. To determine whether apoptosis induction can also be found in primary human cells, we incubated **2** and **3** with leukemia cells taken from a patient with relapsed childhood ALL. The isolated primary lymphoblasts were treated with **2** and **3** at the ID_{50} concentrations established for BJAB cells and with the cytostatic drugs daunorubicin, doxorubicin, and vincristine. As can be gauged from Figure 11, complexes **2** and **3** appear to exhibit superior apoptosis induction relative to these standard drugs for the treatment of childhood ALL.

Our investigations also clearly demonstrate that complexes **2** and **3** trigger the mitochondrial pathway of apoptosis. As illustrated in Figure 12 a, dose-dependent loss of the mitochondrial membrane potential was observed for BJAB cells after 48 h incubation with the meridional rhodium(III) compounds. This was also the case for the iridium(III) complexes **11** and **14** (Figure 12 b). After staining the cells with the dye JC-1 (5,5′,6,6′-tetrachloro-1,1,3,3′-tetraethylbenzimidazolylcarbocyanine iodide), mitochondrial permeability was quantified by flow cytometric determination of the cells with decreased fluorescence, that is, with mitochondria displaying a lower membrane potential.

Conclusions

The meridional rhodium(III) polypyridyl complexes of the type *mer*-[RhX_3(DMSO)(pp)] (X = Cl, Br) represent a highly promising class of potent cytostatic agents. In extension of our previous in vitro studies on breast cancer (MCF-7) and colon carcinoma cells (HT-29),[10] the present work now establishes the considerable potential of the polypyridyl complexes *mer*-[$RhCl_3$(DMSO)(dpq)] **2** and *mer*-[$RhCl_3$(DMSO)(dppz)] **3** for the treatment of lymphoma and leukemia. Following the publication of our original results for the series *mer*-[$RhCl_3$(DMSO)(pp)] (pp = bpy, phen, dpq, dppz, dppn), a report on the cytostatic activity of *fac*-[$RhCl_3$(DMSO)(bpy)]·DMSO and *mer*-[$RhCl_3$(DMSO)(phen)]·DMSO toward Caco-2 (colon adenocarcinoma) and

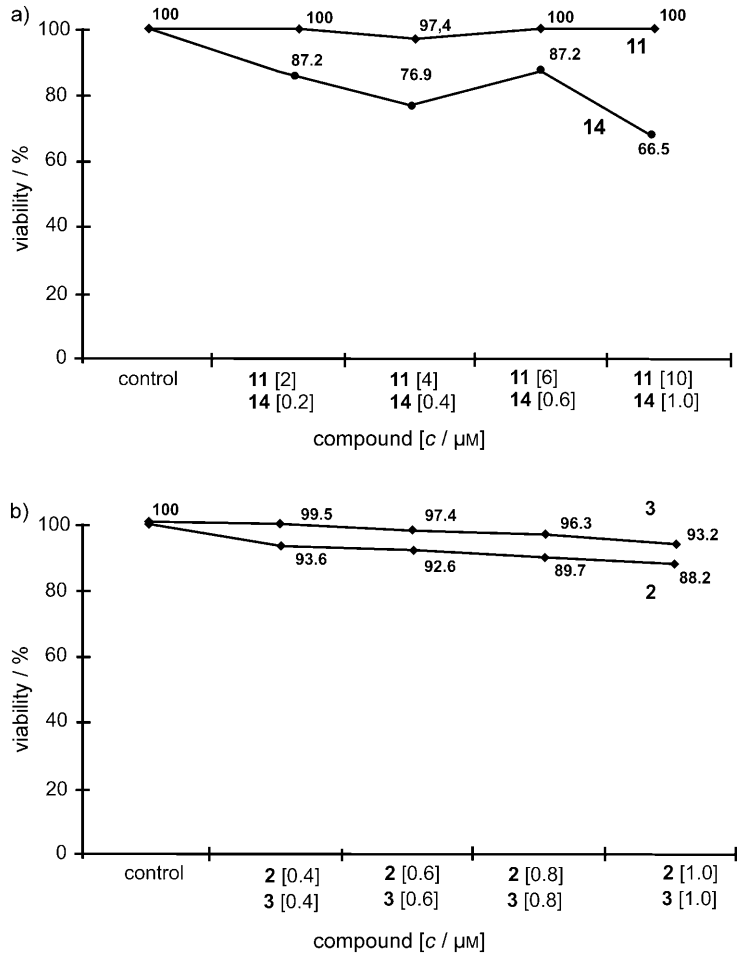

Figure 9. a) Detection of significant necrosis for BJAB cells in the presence of complex **14** relative to the unspecific cytotoxic effects observed for complex **11.** b) Cell viability values for complexes **2** and **3**; viability was determined using the LDH release assay after an incubation period of 1 h for complexes **11** and **14** and 3 h for complexes **2** and **3**.

A549 (lung adenocarcinoma) has also very recently appeared.[23] In accordance with the trends listed in Table 1, the meridional phen complex is more active toward these cell lines (IC_{50}: 0.67 ± 0.05 and 0.38 ± 0.04 μM) than the facial bpy complex (IC_{50}: 1.19 ± 0.05 and 12.58 ± 0.50 μM).

Our current studies demonstrate that both the meridional rhodium(III) complexes *mer*-[$RhCl_3$(DMSO)(pp)] (pp = dpq **2**, dppz **3**) and the facial iridium(III) complex *fac*-[$IrCl_3(H_2O)$(phen)] **11** induce apoptosis via the intrinsic mitochondrial pathway. In contrast to the likewise apoptosis-inducing complex *mer*-[$IrCl_3$(tpy)] **14**, necrotic cell death appears to be negligible for the complexes of the general type [MCl_3(L)(pp)]. Complexes **2** and **3** exhibit superior apoptosis induction in comparison with the standard drugs daunorubicin, doxorubicin, and vincristine for the treatment of childhood acute lymphoblastic leukemia.

The synthesis and cytotoxicity studies of the analogous ruthenium(III) complexes *mer*-[$RuCl_3$(DMSO)(dpq)] and *mer*-[$RuCl_3(CH_3CN)$(dpq)] have also been recently reported.[24] Despite their apparent structural analogy to the complexes **1**–**4** and **7** and **8**, these Ru^{III} compounds can be regarded as effectively inactive on the basis of their very high IC_{50} values of ~600–800 μM toward the cell lines MCF-7, SCG-7901 (gastric cancer), BEL-7402 (hepatic cancer), CNE-2 (nasopharyngeal carcinoma), and HELA (cervical cancer). The establishment of the structure–activity series Ru ≪ Ir < Rh for complexes of the type *mer*-[MCl_3(L)(pp)] suggests that the rate of chloride and/or ligand L substitution may be decisive in determining their cytotoxicity for a particular polypyridyl ligand. Whereas one or two of its chloride ions are rapidly replaced by aqua ligands, this is not the case for the DMSO ligand in *mer*-[$RuCl_3$(DMSO)(dpq)].[24] The resulting cationic species not only intercalate into DNA but also react rapidly with bovine serum albumin, which suggests that their very low cytotoxicity may be due to rapid and strong covalent binding to biomolecules other than the potential target molecules in the cell. In contrast, relatively rapid DMSO/H_2O exchange is observed for *mer*-[$RhCl_3$(DMSO)(pp)],[10] and the resulting neutral aqua complexes appear to exhibit neither intercalation nor covalent binding to DNA. The iridium(III) complexes *fac*-[$IrCl_3$(DMSO)(pp)] are highly inert, and no significant DMSO/H_2O or Cl^-/H_2O substitution is observed for their aqueous solutions.[11] Like the meridional Rh^{III} complexes, neither intercalative nor covalent interactions with DNA can be detected, but the soft Ir^{III} compounds do react slowly with biomolecules containing S donor atoms, such as *N*-acetylmethionine. Taking all these facts into account, it can be postulated that the rate and nature of the ligand substitution reactions for the Rh^{III} complexes may indeed be favorable for high cytotoxicity, whereas the lower activities of the analogous Ir^{III} and Ru^{III} compounds may be due to their respectively much higher or much lower kinetic stabilities.

The striking differences between the activities of the meridional and facial isomers may also be the result of differing kinetic stabilities that could influence the extent of cellular uptake, which is much higher for *mer*-[$RhCl_3$(DMSO)(pp)][10] than for *fac*-[$IrCl_3$(DMSO)(pp)].[11] Our present results indicate that there is still much scope for tuning the activities of this novel class of cytotoxic compounds [MCl_3(L)(pp)] (M = Rh, Ir) by varying both the coordination geometry (*mer* vs. *fac*) and the combination of ligands (X, L, pp).

Experimental Section

Chemistry

Materials and instrumentation: UV/Vis spectra were recorded with an Analytik Jena SPECORD 200 spectrometer. A Jasco J-715 instrument was used to measure CD spectra in the range 220–500 nm for 1:10 complex/DNA mixtures [complex = 20 μM, DNA concentration in M(nucleotide) = 200 μM] in a 10 mM phosphate buffer at pH 7.2. LSIMS (liquid secondary ion mass spectrometry) data were registered with a Fisons VG Autospec employing a cesium ion gun (17 kV) and 3-nitrobenzyl alcohol as the liquid matrix. Bruker DPX 200 and DRX 400 spectrometers were used for

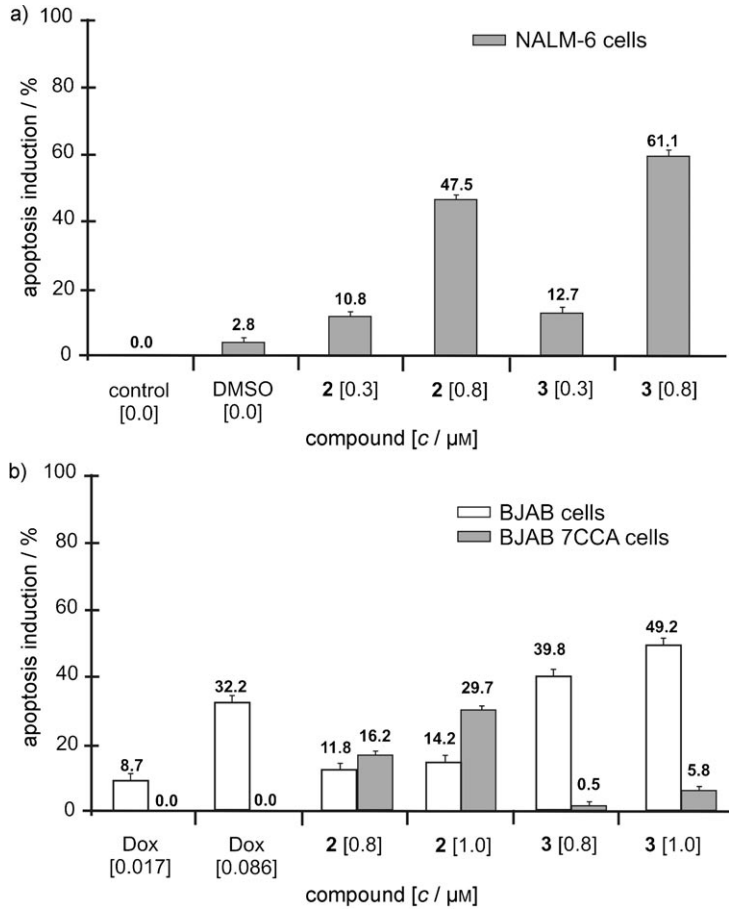

Figure 10. Apoptosis induction as measured by DNA fragmentation in a) leukemia cells (NALM-6) and b) lymphoma cells (regular BJAB and doxorubicin-resistant BJAB cells = -Doxo7CCA) after treatment for 72 h with various concentrations of **2**, **3**, and doxorubicin (Dox). Data are given in percent hypoploidy (sub-G_1) ± ESD ($n = 3$), which reflects the number of apoptotic cells.

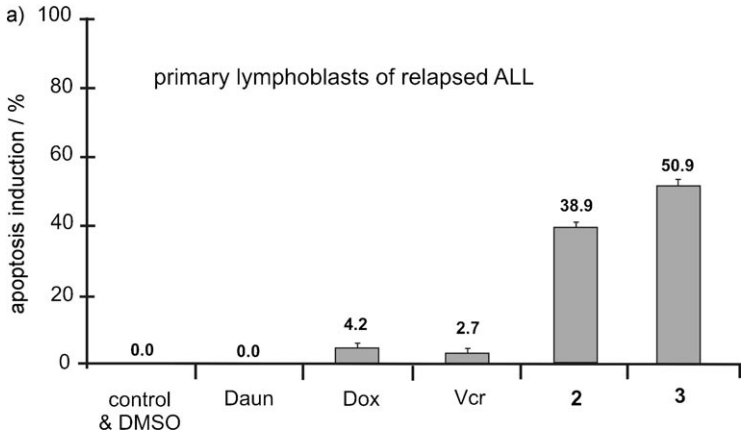

Figure 11. Apoptosis induction as measured by DNA fragmentation in primary leukemia cells isolated from a patient with relapsed childhood ALL after treatment for 60 h with **2**, **3**, and standard cytostatic agents in clinical use (Daun = daunorubicin, Dox = doxorubicin, Vcr = vincristine). All cytostatic agents were applied at the LC_{50} concentrations determined for BJAB cells. Data are given in percent hypoploidy (sub-G_1) ± ESD ($n = 3$), which reflects the number of apoptotic cells.

^{1}H NMR spectroscopy, with chemical shifts reported as δ values relative to the signal of tetramethylsilane. Elemental analyses were performed on a Vario EL instrument (Elementar Analysensysteme, Jena, Germany). $RhX_3 \cdot 3H_2O$ and $IrX_3 \cdot 3H_2O$ (X = Cl, Br) were purchased from Chempur, phen, tpy, 1-methylimidazole, and 1-methylbenzimidazole from Acros, and dimethyl sulfoxide (DMSO) from J. T. Baker. The polypyridyl ligand dpq[25] was prepared in accordance with published procedures as were the complexes *mer*-[$RhCl_3$(DMSO)(pp)] (pp = phen, dpq, dppz, **1**–**3**).[10]

X-ray structural analyses: Intensity data were collected with an Oxford Diffraction Xcalibur2 diffractometer equipped with a Sapphire-CCD using 1° ω scans and $Mo_{K\alpha}$ radiation ($\lambda = 0.71073$ Å). The data were corrected for absorption by the Gauss method and solved by direct methods with SHELX97. Refinement against F_0^2 was performed by SHELXL97[26] with anisotropic temperature factors for non-hydrogen atoms, and protons as riding atoms at geometrically calculated positions. CCDC 701113, 701114, and 701115 contain the supplementary crystallographic data for this paper. These data can be obtained free of charge from The Cambridge Crystallographic Data Centre via www.ccdc.cam.ac.uk/data_request/cif.

***mer*-[$RhBr_3$(DMSO)(phen)] (4):** $RhBr_3 \cdot 3H_2O$ (200.0 mg, 0.54 mmol) was heated in 1 mL DMSO at 70 °C for 4 h. After addition of cold EtOH the solution was left to stand at −18 °C to afford [$RhBr_3(DMSO)_3$] as a red-brown precipitate, which was filtered off and dried under vacuum before further use. 1,10-Phenanthroline (34.5 mg, 0.17 mmol) was then added to [$RhBr_3(DMSO)_3$] (100.0 mg, 0.17 mmol) in CH_3OH (10 mL), and the reaction mixture was heated at 70 °C for 2 h. The resulting solid was filtered off, washed with CH_3OH and Et_2O and dried in vacuum. Yield: 49 mg (48%); ^{1}H NMR (200 MHz, [D_6]DMSO): $\delta = 3.95$ (s, 6H, DMSO), 8.25–8.38 (m, 2H, H3/H8), 8.42 (d, 2H, H5/H6), 9.01 (d, 1H, H4), 9.08 (d, 1H, H7), 10.21 (d, 1H, H2), 10.26 ppm (d, 1H, H9); LSIMS: *m/z* (%): 522(69) $[M-Br]^+$, 443(36) $[M-Br-DMSO]^+$, 364(100) $[M-2Br-DMSO]^+$, 283(21) $[M-3Br-DMSO]^+$; Anal. calcd for $C_{14}H_{14}BrN_2ORhS$ ($M = 601.0$): C 28.0%, H 2.3%, N 4.7%, S 5.3%, found: C 27.9%, H 2.3%, N 4.7%, S 5.2%.

***mer*-[$IrCl_3$(DMSO)(phen)] (7):** $IrCl_3 \cdot 3H_2O$ (176.3 mg, 0.5 mmol) and DMSO (36 μL, 0.5 mmol) were dissolved in CH_3OH (25 mL) and heated for 2 h at 80 °C. After solvent removal, *N*,*N*-dimethylformamide (DMF, 25 mL) and 1,10-phenanthroline (99.1 mg, 0.5 mmol) were added to the residue, and the reaction mixture was heated at 120 °C for 2 h. Following cooling to 25 °C and renewed solvent removal, the resulting solid was dissolved in CH_3OH (2 mL), and the product was precipitated by addition of Et_2O and dried under vacuum. Yield: 210.2 mg (75%); ^{1}H NMR (200 MHz, $CDCl_3$): $\delta = 3.78$ (s, 6H, DMSO), 7.92 (dd, 1H, H3), 8.01 (dd, 1H, H8), 8.06 (d, 2H, H5/H6), 8.43 (d, 1H, H4), 8.56 (d, 1H, H7), 10.12 (d, 1H, H2), 10.39 ppm (d, 1H, H9); LSIMS: *m/z* (%): 521(10) $[M-Cl]^+$, 480(7) $[M-DMSO]^+$, 445(37) $[M-Cl-DMSO]^+$, 409(12) $[M-2Cl-DMSO]^+$; Anal. calcd for $C_{14}H_{14}Cl_3IrN_2OS$ ($M = 556.9$): C 30.2%, H 2.5%, N 5.0%, found: C 29.8%, H 2.5%, N 5.1%.

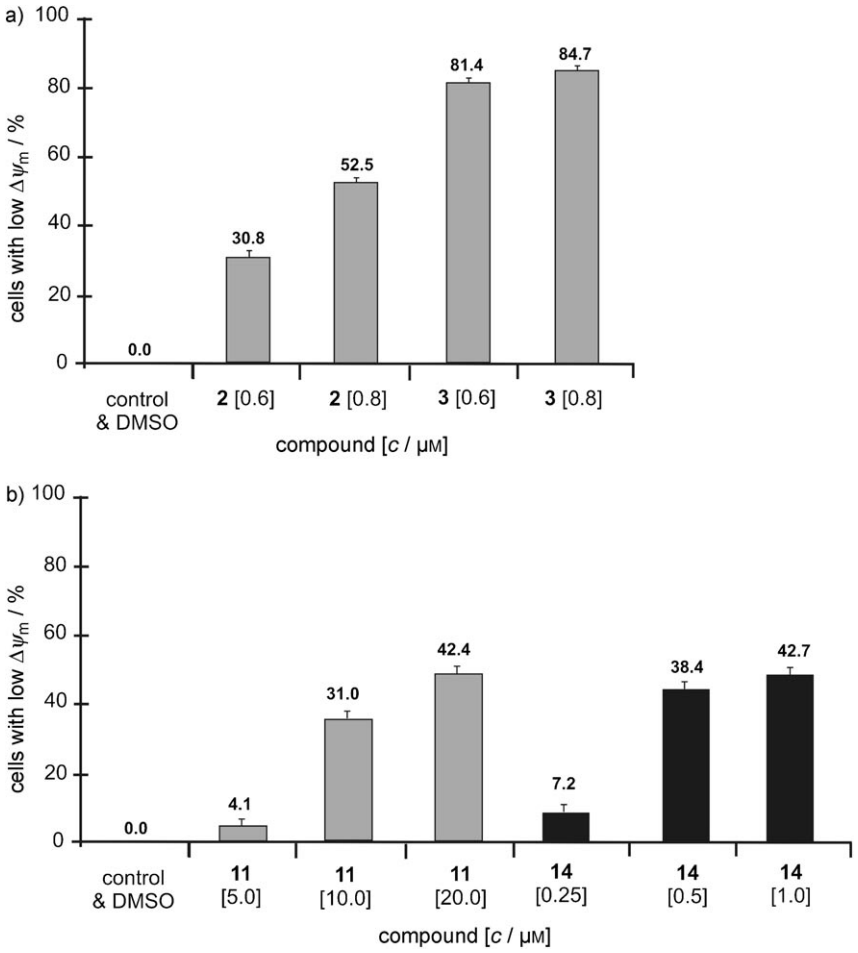

Figure 12. Mitochondrial permeability transition as measured by flow cytometric analysis in lymphoma cells (BJAB) after treatment with various concentrations of a) **2** and **3**, and b) **11** and **14** for 48 h. Values of the mitochondrial permeability transition are given as the percentage of cells with low $\Delta\psi_m$ ±ESD ($n=3$).

***mer*-[IrBr$_3$(DMSO)(phen)] (8):** Preparation as for **7** with 215.9 mg $IrBr_3{\cdot}3H_2O$ (0.5 mmol). Yield: 223.4 mg (65%); ^{1}H NMR (200 MHz, CD_2Cl_2): $\delta=3.95$ (s, 6H, DMSO), 7.90 (dd, 1H, H3), 8.00 (dd, 1H, H8), 8.05 (d, 2H, H5/H6), 8.44 (d, 1H, H4), 8.54 (d, 1H, H7), 10.28 (d, 1H, H2), 10.39 ppm (d, 1H, H9); LSIMS: *m/z* (%): 690(5) $[M]^+$, 611(15) $[M-Br]^+$, 531(17) $[M-2Br]^+$; Anal. Calcd for $C_{14}H_{14}Br_3IrN_2OS$ ($M=690.3$): C 24.4%, H 2.0%, N 4.1%, found: C 24.0%, H 2.1%, N 4.1%.

***fac*-[IrCl$_3$(H$_2$O)(phen)] (9):** $IrCl_3{\cdot}3H_2O$ (105.8 mg, 0.3 mmol) and 1,10-phenanthroline (54.0 mg, 0.3 mmol) were dissolved in 10 mL H_2O and heated for 4 h at 110 °C. Following cooling to 25 °C and solvent removal under vacuum, the resulting solid was washed with CH_3OH and Et_2O and dried under vacuum. Yield: 78.9 mg (53%); ^{1}H NMR (200 MHz, CD_3OD): $\delta=3.49$ (s, 2H, H_2O), 7.76 (dd, 2H, H3/H8), 7.94 (s, 2H, H5/H6), 8.46 (dd, 2H, H4/H7), 9.05 ppm (dd, 2H, H2/H9); LSIMS: *m/z* (%): 478(1) $[M-H_2O]^+$, 443(7) $[M-H_2O-Cl]^+$; Anal. calcd for $C_{12}H_{10}Cl_3IrN_2O$ ($M=496.8$): C 29.0%, H 2.0%, N 5.6%, found: C 28.6%, H 2.0%, N 5.6%.

***fac*-[IrCl$_3$(H$_2$O)(dpq)]·H$_2$O (10):** Preparation as for **9** with dipyrido[3,2-*f*:2′,3′-*h*]quinoxaline (69.6 mg, 0.3 mmol). Yield: 76.5 mg (45%); ^{1}H NMR (200 MHz [D$_6$]DMSO): $\delta=7.97$ (m, 2H, H3/H8), 9.19 (s, 2H, H11/H12), 9.25 (d, 2H, H4/H7), 9.45 ppm (d, 2H, H2/H9); LSIMS: *m/z* (%): 517(1) $[M-H_2O-Cl+Na]^+$, 482(3) $[M-H_2O-2Cl+Na]^+$; Anal. calcd for $C_{14}H_{12}Cl_3IrN_4O_2$ ($M=566.9$): C 29.7%, H 2.1%, N 9.9%, found: C 29.3%, H 2.1%, N 10.2%.

***fac*-[IrBr$_3$(H$_2$O)(phen)]·2 H$_2$O (11):** Preparation as for **9** with $IrBr_3{\cdot}3H_2O$ (291.6 mg, 0.6 mmol) and *o*-phenanthroline (108.1 mg, 0.6 mmol). Yield: 315.3 mg (83%); ^{1}H NMR (200 MHz, CD_3OD): $\delta=$ 3.51 (s, 2H, H_2O), 7.79 (dd, 2H, H3/H8), 7.97 (s, 2H, H5/H6), 8.49 (dd, 2H, H4/H7), 9.09 ppm (dd, 2H, H2/H9); LSIMS: *m/z* (%): 648(3) $[M-H_2O]^+$, 568(1) $[M-H_2O-Br]^+$; Anal. calcd for $C_{12}H_{14}Br_3IrN_2O_3$ ($M=666.2$): C 21.6%, H 2.1%, N 4.2%, found: C 21.8%, H 1.7%, N 4.2%.

***fac*-[IrBr$_3$(1-MeIm)(phen)] (12):** 1-Methylimidazole (1-MeIm) (16 μL, 0.2 mmol) was added to *fac*-[$IrBr_3$-(H_2O)(phen)]·3H_2O **5** (123.8 mg, 0.2 mmol) in CH_3OH (10 mL) and the mixture was held at reflux for 2 h. Following cooling to 25 °C and solvent removal under vacuum, H_2O/CH_3OH (1:1 *v/v*, 10 mL) was added to the resulting solid, and the mixture was heated for 72 h at 80 °C. After renewed solvent removal, the product was washed with CH_3OH and Et_2O and dried under vacuum. Yield: 50.3 mg (36%); ^{1}H NMR (200 MHz, CD_2Cl_2): $\delta=3.89$ (s, 3H, CH_3), 7.14 (d, 1H, 1-MeIm H), 7.38 (d, 1H, 1-MeIm H), 7.69 (dd, 2H, H3/H8) 7.86 (s, 2H, H5/H6), 8.33 (dd, 2H, H4/H7), 8.52 (s, 1H, 1-MeIm H), 9.18 ppm (dd, 2H, H2/H9); LSIMS: *m/z* (%): 697(8) $[M]^+$, 617(10) $[M-Br]^+$; Anal. calcd for $C_{16}H_{14}Br_3IrN_4$ ($M=694.2$): C 27.7%, H 2.0%, N 8.1%, found: C 27.4%, H 2.2%, N 8.5%.

***fac*-[IrBr$_3$(1-MeBIm)(phen)]·H$_2$O (13):** Preparation as for **12** with 1-methylbenzimidazole (26.4 mg, 0.2 mmol). Yield: 59.5 mg (39%); ^{1}H NMR (200 MHz, CD_2Cl_2): $\delta=1.24$ (s, 3H, CH_3), 7.51 (m, 3H, MeBIm H), 7.69 (dd, 2H, H3/H8) 7.83 (s, 2H, H5/H6), 7.97 (d, 1H, MeBIm H), 8.31 (dd, 2H, H4/H7), 9.23 (dd, 2H, H2/H9), 9.57 (s, 1H, MeBIm H); LSIMS: *m/z* (%): 665(6) $[M-Br]^+$; Anal. calcd for $C_{20}H_{18}Br_3IrN_4O$ ($M=762.3$): C 31.5%, H 2.4%, N 7.3%, found: C 31.4%, H 2.3%, N 7.3%.

***mer*-[IrCl$_3$(tpy)]·3 H$_2$O (14):** $IrCl_3{\cdot}3H_2O$ (70.5 mg, 0.2 mmol) and 2,2′:6′,2″-terpyridine (46.6 mg, 0.2 mmol) were heated for 2 h at 80 °C in CH_3OH (10 mL). After cooling to 25 °C and solvent removal under vacuum, the resulting solid was washed with CH_3OH and Et_2O and dried under vacuum. Yield: 98.0 mg (92%); ^{1}H NMR (400 MHz, [D$_6$]DMSO): $\delta=7.59$ (dd, 2H, H2/H2′), 8.11 (dd, 2H, H3/H3′), 8.15 (t, 1H, H6), 8.49 (d, 2H, H5/H5′) 8.77 (d, 2H, H1/H1′); LSIMS: *m/z* (%): 496(5) $[M-Cl]^+$, 461(6) $[M-2Cl]^+$; Anal. calcd for $C_{15}H_{11}Cl_3IrN_3$ ($M=531.8$): C 30.7%, H 2.9%, N 7.2%, found: C 30.3%, H 2.7%, N 6.8%.

***mer*-[IrBr$_3$(tpy)]·3 H$_2$O (15):** Preparation as for **14** with $IrBr_3 \cdot 3H_2O$ (97.2 mg, 0.2 mmol). Yield: 108.4 mg (81%); ^{1}H NMR (400 MHz, [D$_6$]DMSO): $\delta = 7.50$ (dd, 2H, H2/H2′), 8.01 (dd, 2H, H3/H3′), 8.11 (t, 1H, H6), 8.45 (d, 2H, H5/H5′) 8.73 ppm (d, 2H, H1/H1′); Anal. calcd for $C_{15}H_{11}Br_3IrN_3$ ($M = 665.2$): C 25.1%, H 2.4%, N 5.8%, found: C 25.2%, H 2.2%, N 5.8%.

Biological investigations

Materials: RNase A was obtained from Qiagen (Hilden, Germany), propidium iodide from Serva (Heidelberg, Germany), and JC-1 from Molecular Probes, Invitrogen (Karlsruhe, Germany).

Cell cultures: MCF-7 breast cancer and HT-29 human colon carcinoma cells were maintained in 10% (*v*/*v*) fetal calf serum (FCS) containing cell culture medium [minimum essential Eagle's supplemented with $NaHCO_3$ (2.2 g), sodium pyruvate (110 mg L^{-1}), and gentamicin sulfate (50 mg L^{-1}) adjusted to pH 7.4] at 37 °C under 5% CO_2, and were passaged twice a week according to standard procedures. BJAB (Burkitt-like lymphoma) and NALM-6 (human B cell precursor leukemia) cells were maintained at 37 °C in RPMI 1640 (GIBCO, Invitrogen) supplemented with 10% heat-inactivated FCS, penicillin (100 000 U L^{-1}), streptomycin (0.1 g L^{-1}), and L-glutamine (0.56 g L^{-1}). The cells were subcultured every 3–4 days by dilution of the cells to a concentration of 1×10^5 cells mL^{-1}. Twenty-four hours before the assay setup, cells were cultured at a concentration of 3×10^5 cells mL^{-1} to ascertain standardized growth conditions. For apoptosis assays, the cells were then diluted to a concentration of 1×10^5 cells mL^{-1} immediately before addition of the various complexes. To generate 7CCA (doxorubicin-resistant BJAB) cells, BJAB cells were exposed to an initial concentration of 0.1 μg L^{-1} doxorubicin and then treated with doxorubicin up to 1 mg L^{-1}, whenever the vitality of the cells was >85%.

Patients: Primary lymphoblasts were obtained by bone marrow aspiration of patients with relapsed acute lymphoblastic leukemia (ALL). The diagnosis was established by immunophenotyping of leukemia cells according to Béné et al.[27] Lymphoblasts and mononuclear cells were separated by centrifugation over Biocoll (Biochrom KG, Berlin, Germany). After separation, the percentage of leukemia cells was >95%. The leukemia cells were immediately seeded at a density of 3×10^5 cells mL^{-1} in RPMI 1640 complete cell culture medium and incubated for 60 h with daunorubicin, doxorubicin, and vincristine, as well as with complexes **1** and **2** at their LD_{50} concentrations in BJAB cells. The use of the cells is in accordance with the ethical standards of the Responsible Committee on Human Experimentation and the Helsinki Declaration as revised in 2000. It is also in accordance with the positive vote of the ethics committee from December 14, 2000 for the ALL-REZ-BFM study in 2002. Informed signed consent was obtained from either the patient or from their next of kin.

Cytotoxicity measurements: The antiproliferative effects of complexes **1**–**15** toward MCF-7 and HT-29 cells were determined by an established procedure.[28] Cells were suspended in cell culture medium (MCF-7: 10 000 cells mL^{-1}; HT-29: 2850 cells mL^{-1}), and aliquots thereof were plated in 96-well plates and incubated at 37 °C under 5% CO_2 for 72 h (MCF-7) or 48 h (HT-29). Stock solutions of the compounds in DMSO or DMF were freshly prepared and diluted with cell culture medium to the desired concentrations (final DMSO or DMF concentration: 0.1% *v*/*v*). The medium in the plates was replaced with the medium containing the compounds in graded concentrations (six replicates). After further incubation for 96 h (MCF-7) or 72 h (HT-29), the cell biomass was determined by crystal violet staining, and the IC_{50} values were established as the concentrations that cause 50% inhibition of cell proliferation. Results were calculated from 2–3 independent experiments.

The cytotoxicity of **2**, **3**, **11**, and **14** toward BJAB cells was measured by release of lactate dehydrogenase (LDH) as described previously.[29] After incubation with various concentrations of the complexes for 1 or 3 h at 37 °C, LDH activity released by BJAB cells was measured in the cell culture supernatants using the Cytotoxicity Detection Kit from Boehringer Mannheim (Mannheim, Germany). The supernatants were centrifuged at 1500 rpm for 5 min. Cell-free supernatants (20 μL) were diluted with phosphate-buffered saline (PBS, 80 μL), and a reaction mixture containing 2-[4-iodophenyl]-3-[4-nitrophenyl]-5-phenyltetrazolium chloride (INT), sodium lactate, oxidized nicotinamide adenine dinucleotide (NAD^+) and diaphorase (100 μL) was added. Time-dependent formation of the reaction product was the quantified photometrically at 490 nm. The maximum amount of LDH activity released by the cells was determined by lysis of the cells with 0.1% Triton X-100 in culture medium, and was set as 100% cell death.

Determination of cell viability: Cell viability was determined by using the CASY Cell Counter and Analyzer System from Innovatis (Bielefeld, Germany). Settings were specifically defined for the requirements of the cells used. With this system, the cell concentration can be analyzed simultaneously in three different size ranges: cell debris, dead cells, and viable cells. Cells were seeded at a density of 1×10^5 cells mL^{-1} and treated with various concentrations of **2**, **3**, **11**, and **14**; non-treated cells served as controls. After a 24 h incubation period at 37 °C, cells were resuspended properly and 100 μL of each well was diluted in 10 mL CASYton (ready-to-use isotonic saline solution) for an immediate automated count of the cells.

Measurement of DNA fragmentation: Apoptotic cell death was determined by a modified cell-cycle analysis, which detects DNA fragmentation at the single-cell level as described previously.[22] Cells were seeded at a density of 1×10^5 cells mL^{-1} and treated with various concentrations of **2**, **3**, **11**, and **14**. After a 72 h incubation period at 37 °C, cells were collected by centrifugation at 1500 rpm for 5 min, washed with PBS at 4 °C, and fixed in PBS/formaldehyde (2% *v*/*v*) on ice for 30 min. After fixation, cells were pelleted, incubated with EtOH/PBS (2:1 *v*/*v*) for 15 min, pelleted, and resuspended in PBS containing 40 μg mL^{-1} RNase A. RNA was digested for 30 min at 37 °C, after which the cells were pelleted once again and finally resuspended in PBS containing 50 μg mL^{-1} propidium iodide. Nuclear DNA fragmentation was quantified by flow cytometric determination of hypodiploid DNA (fluorescence-activated cell sorting, FACS). Data were collected and analyzed using a FACScan (Becton Dickinson, Heidelberg, Germany) apparatus equipped with CELL Quest software. Data are given in percent hypoploidy (sub-G_1), which reflects the number of apoptotic cells.

Measurement of the mitochondrial permeability transition: After an incubation period of 48 h with various concentrations of **2**, **3**, **11**, and **14**, cells were collected by centrifugation at 1500 rpm, 4 °C for 5 min. The mitochondrial permeability transition was then determined by staining the cells with 5,5′,6,6′-tetrachloro-1,1′,3,3′-tetraethylbenzimidazolylcarbocyanine iodide (JC-1; Molecular Probes, Leiden, The Netherlands). 1×10^5 cells were resuspended in 500 μL phenol-red-free RPMI 1640 without supplements, and JC-1 was added to give a final concentration of 2.5 μg mL^{-1}. The cells were incubated for 30 min at 37 °C with moderate shaking. Control cells were likewise incubated in the absence of JC-1 dye. The cells were harvested by centrifugation at 1500 rpm, 4 °C for 5 min, washed with ice-cold PBS, and resuspended in 200 μL PBS at 4 °C. Mito-

chondrial permeability transition was then quantified by flow cytometric determination of the cells with decreased fluorescence, that is, with mitochondria displaying a lower membrane potential. Data were collected and analyzed using a FACScan (Becton Dickinson, Heidelberg, Germany) apparatus equipped with CELL Quest software. Data are given in percentage of cells with low $\Delta\Psi_m$, which reflects the number of cells undergoing mitochondrial apoptosis.

Fluorescence microscopy: Microscopic work was performed with an Axioskop2 with the fluorescence option from Zeiss, equipped with the set of filters 09, with $\lambda_{ex}=450$–490 nm and $\lambda_{em}=515$ nm. BJAB cells were incubated with **3** for 12 h at 37 °C and subsequently fixed with formaldehyde. The fixed cells (20 μL) were applied to a slide with poly-L-lysine (Sigma) into a painted circle (Kisker). After a careful drying process, the fixed cells were washed twice with PBS. Afterward the BisBenzimid H 33258 (Sigma) coloring agent was applied in a diluted concentration of 0.25 μg mL^{-1} PBS. BisBenzimid colors and displays the nuclei of treated cells. Before the microscopy studies, the slides were treated with glycerin (Sigma) and kept in the dark at 4 °C.

Acknowledgements

Financial support for this work in Berlin and Bochum by the Deutsche Forschungsgemeinschaft (DFG) within the research group FOR 630 "Biological function of organometallic compounds" is gratefully acknowledged. We also thank Corazon Frias, Heike Scheffler, and Manuela Winter for excellent technical support.

Keywords: apoptosis · cytotoxicity · iridium · polypyridyl ligands · rhodium

[1] N. Katsaros, A. Anagnostopoulou, *Crit. Rev. Oncol. Hematol.* **2002**, *42*, 297–308.
[2] A. M. Angeles-Boza, H. T. Chifotides, J. D. Aguirre, A. Chouai, P. K. L. Fu, K. R. Dunbar, C. Turro, *J. Med. Chem.* **2006**, *49*, 6841–6847.
[3] P. Qu, H. He, X. Liu, *Prog. Chem.* **2006**, *18*, 1646–1651.
[4] G. Mestroni, E. Alessio, A. Sessanti o Santi, S. Geremia, A. Bergamo, G. Sava, A. Boccarelli, A. Schettino, M. Coluccia, *Inorg. Chim. Acta* **1998**, *273*, 62–71.
[5] D. A. Medvetz, K. D. Stakleff, T. Schreiber, P. D. Custer, K. Hindi, M. D. Panzner, D. D. Blanco, M. J. Taschner, C. A. Tessier, W. J. Youngs, *J. Med. Chem.* **2007**, *50*, 1703–1706.
[6] F. P. Pruchnik, P. Jakimowicz, Z. Ciunik, J. Zakrzewska-Czerwińska, A. Opolski, J. Wietrzyk, E. Wojdat, *Inorg. Chim. Acta* **2002**, *324*, 59–66.
[7] M. A. Scharwitz, I. Ott, Y. Geldmacher, R. Gust, W. S. Sheldrick, *J. Organomet. Chem.* **2008**, *693*, 2299–2309.
[8] S. Schäfer, W. S. Sheldrick, *J. Organomet. Chem.* **2007**, *692*, 1300–1309.
[9] S. Schäfer, I. Ott, R. Gust, W. S. Sheldrick, *Eur. J. Inorg. Chem.* **2007**, 3034–3046.
[10] M. Harlos, I. Ott, R. Gust, H. Alborzinia, S. Wölfl, A. Kromm, W. S. Sheldrick, *J. Med. Chem.* **2008**, *51*, 3924–3933.
[11] M. A. Scharwitz, I. Ott, R. Gust, A. Kromm, W. S. Sheldrick, *J. Inorg. Biochem.* **2008**, *102*, 1623–1630.
[12] B. R. James, R. H. Morris, *Can. J. Chem.* **1980**, *58*, 399–408.
[13] E. Alessio, P. Faleschini, A. Sessanti o Santi, G. Mestroni, M. Calligaris, *Inorg. Chem.* **1993**, *32*, 5756–5761.
[14] E. D. McKenzie, R. A. Plowman, *J. Inorg. Nucl. Chem.* **1970**, *32*, 199–212.
[15] J. A. Broomhead, W. Grumley, *Inorg. Chem.* **1971**, *10*, 2002–2009.
[16] X-ray structural analysis of *fac*-[IrCl$_3$(CH$_3$CN)(phen)] **9a**: $M=560.86$, triclinic $P\bar{1}$, $a=7.159(1)$, $b=10.234(1)$, $c=12.860(1)$ Å, $\alpha=92.48(1)$, $\beta=98.46(1)$, $\gamma=110.25(1)^\circ$, $V=869.74(6)$ Å^3, $T=120$ K, $Z=4$, $d_{calcd}=2.142$ g cm^{-3}, $\mu=8.142$ mm^{-1}. A total of 6952 reflections were measured, of which 3040 were unique ($R_{int}=0.026$) and 2664 had $I>2\sigma(I)$. Final residuals were $R_1=0.022$ (for $I>2\sigma(I)$), $wR_2=0.0470$ (for all data), and GOOF = 0.956, with a largest residual peak 1.36 e A^{-3}, and a largest residual hole of -1.00 e A^{-3}.
[17] X-ray structural analysis for *mer*-[IrCl$_3$(tpy)] **14**: $M=531.82$, monoclinic $P2_1/n$, $a=8.264(1)$, $b=14.020(1)$, $c=13.647(1)$ Å, $\beta=105.07(1)$, $V=1526.74(7)$ Å^3, $T=120$ K, $Z=4$, $d_{calcd}=2.314$ g cm^{-3}, $\mu=9.267$ mm^{-1}; 10600 measured reflections with 2678 unique ($R_{int}=0.016$) and 2270 with $I>2\sigma(I)$. Final residuals were $R_1=0.016$ for $I>2\sigma(I)$, $wR_2=0.033$ (all data) and GOOF = 1.020, with a largest residual peak of 1.31 e A^{-3}, and a largest residual hole of -0.62 e A^{-3}.
[18] X-ray structural analysis for *mer*-[IrBr$_3$(tpy)] **15**: $M=665.20$, monoclinic $P2_1/n$, $a=8.438(1)$, $b=14.363(1)$, $c=13.957(1)$ Å, $\beta=106.42(1)$, $V=1622.5(2)$ Å^3, $T=120$ K, $Z=4$, $d_{calcd}=2.723$ g cm^{-3}, $\mu=15.615$ mm^{-1}; 7036 measured reflections with 2830 unique ($R_{int}=0.117$) and 1187 with $I>2\sigma(I)$. Final residuals were $R_1=0.047$ for $I>2\sigma(I)$, $wR_2=0.099$ (all data) and GOOF = 0.558, with a largest residual peak of 1.89 e A^{-3}, and a largest residual hole of -1.07 e A^{-3}.
[19] T. Poth, H. Paulus, H. Elias, C. Dücker-Benfer, R. van Eldik, *Eur. J. Inorg. Chem.* **2001**, 1361–1369.
[20] F. Wang, A. Habtemariam, E. P. L. van der Geer, R. Fernandez, M. Melchart, R. J. Deeth, R. Aird, S. Guichard, F. P. A. Fabbiani, P. Lozano-Casal, I. D. H. Oswald, D. I. Jodrell, S. Parsons, P. J. Sadler, *Proc. Natl. Acad. Sci. USA* **2005**, *102*, 18269–18274.
[21] a) T. Wieder, F. Essmann, A. Prokop, K. Schmelz, K. Schulze-Osthoff, R. Beyaert, B. Dörken, P. T. Daniel, *Blood* **2001** *97*, 1378–1387; b) T. Wieder, C. E. Orfanos, C. C. Geilen, *J. Biol. Chem.* **1998**, *273*, 11025–11031.
[22] T. Wieder, A. Prokop, B. Bagci, F. Essmann, D. Bernicke, K. Schulze-Osthoff, B. Dörken, H.-G. Schmalz, P. T. Daniel, G. Henze, *Leukemia* **2001**, *15*, 1735–1742.
[23] U. Sliwinska, F. P. Pruchnik, I. Pelinska, S. Ulaszewski, A. Wilczok, A. Zajdel, *J. Inorg. Biochem.* **2008**, *102*, 1947–1951.
[24] C. Tan, J. Liu, H. Li, W. Zheng, S. Shi, L. Chen, L. Ji, *J. Inorg. Biochem.* **2008**, *102*, 347–358.
[25] J. G. Collins, A. D. Steemann, J. R. Aldrich-Wright, I. Greguric, T. W. A. Hambley, *Inorg. Chem.* **1998**, *37*, 3133–3141.
[26] G. M. Sheldrick, SHELXS97 and SHELXL97, Göttingen Germany, **1997**.
[27] M. C. Béné, G. Castoldi, W. Knapp, W. D. Ludwig, E. Matutes, A. Orfao, M. B. van't Veer, *Leukemia* **1995**, *9*, 1783–1786.
[28] I. Ott, K. Schmidt, B. Kircher, P. Schuhmacher, T. Wiglenda, R. Gust, *J. Med. Chem.* **2005**, *48*, 622–629.
[29] R. A. Diller, H. M. Riepl, O. Rose, C. Frias, G. Henze, A. Prokop, *Chem. Biodiversity* **2005**, *2*, 1331–1337.

Received: September 24, 2008
Revised: October 29, 2008
Published online on December 19, 2008

